DETAILED INVESTIGATION OF OVERWASH ON A GRAVEL BARRIER

Ana Matias[1], Chris E Blenkinsopp[2], Gerd Masselink[3]

[1] CIMA-Universidade do Algarve, 8000 Faro, Portugal, ammatias@ualg.pt

[2]Department of Architecture and Civil Engineering, University of Bath, Bath, BA2 7AY, United Kingdom, c.blenkinsopp@bath.ac.uk

[3]School of Marine Science and Engineering, University of Plymouth, PL4 8AA, U.K., g.masselink@plymouth.ac.uk

Abstract

This paper uses results obtained from a prototype-scale experiment (Barrier Dynamics Experiment; BARDEX) undertaken in the Delta flume, the Netherlands, to investigate overwash hydraulics and morphodynamics of a prototype gravel barrier. Gravel barrier behaviour depends upon a number of factors, including sediment properties (porosity, permeability, grain-size) and wave climate. Since overwash processes are known to control short-term gravel barrier dynamics and long-term barrier migration, a detailed quantification of overwash flow properties and induced bed-changes is crucial. Overwash hydrodynamics of the prototype gravel barrier focused on the flow velocity, depth and discharge over the barrier crest, and the overwash flow progression across and the infiltration through the barrier. During the BARDEX experiment, overwash peak depth (0.77 m), velocity (5 m s^{-1}) and discharge (max. 6 m^3 m^{-1}) were high, especially considering the

relatively modest wave energy (significant wave height = 0.8 m). Conversely to schemes found in the literature, average flow depth did not linearly decrease across the barrier; rather, it was characterised by a sudden decrease at the crest, a milder decrease at the barrier top and then propagation as a shallow water lens over the backbarrier. The barrier morphological evolution was analysed over a series of 15-min experimental runs and at the timescale of individual overwash events. Overall, the morphological variation did not result from an accumulation of many small consistently erosive or accretionary events, but rather the mean bed elevation change per event was quite large (10 mm) and the overall morphology change occurred due to a small imbalance in the number of erosive and accretionary events at each location. Two relationships between overwash hydrodynamic variables were deduced from results: (1) between overwash flow depth and velocity a power-type relation was obtained; and (2) a linear relation was observed between overwash flow depth and maximum overwash intrusion distance across the barrier top (i.e. overwash intrusion). Findings from this study are useful to enhance the knowledge of overwash processes and also have practical applications. On the one hand, results shown here can be use for the validation of overwash predictive models, and additionally, the simple empirical relations deduced from the dataset can be used by coastal managers to estimate overwash intrusion distance, which in turn can assist in the location of areas under risk of overwash and breaching.

Key-words: BARDEX; storm; bed-level sensors; gravel; barrier; coastal hazards

1. INTRODUCTION

Gravel beaches are widespread on the wave-dominated coastlines of Northern Europe, Canada, USA, Japan, New Zealand and Latin America (Buscombe and Masselink, 2006), and develop in a variety of settings where sediment supply and wave energy favour the accumulation of coarse sediments in the shore zone (Orford et al., 2002). Overwash plays an important role in the evolution of gravel barrier beaches causing them to migrate inland over time by the 'rollover' mechanism (e.g., Orford and Carter, 1982; Carter and Orford, 1993). This mechanism involves onshore-directed sediment transport driven by storm waves through erosion from the front of the barrier, transfer across the barrier crest and deposition at the back of the barrier in the form of washover deposits. By controlling the rate and spatial pattern of gravel barrier rollover, storm waves have been regarded as driving short-term (annual to decadal) gravel barrier migration (Orford et al., 1995). Overwash can also contribute to other patterns of gravel barrier evolution, such as breaching (Bray and Duane, 2001), barrier breakdown (Pye and Blott, 2009), outlet formation (Hart, 2007) and outlet closure (Orford et al., 1988).

Despite the importance of overwash in determining the dynamic behaviour of gravel beaches, field measurements of overwash are scarce. Important field studies on this subject are reported by Orford et al. (1999), Lorang (2002), Orford et al. (2003) and Bradbury et al. (2005), and in the laboratory by Obhrai et al. (2008). Overwash mainly occurs during storms and accurate field measurements are therefore hazardous and difficult to obtain. Overwash sediment transport in sandy beaches has been measured using pre- and post-storm surveys (e.g., Guillén et al., 1994; Stone et al., 2004), and evaluated with ground photographs and vertical or

oblique aerial photographs (e.g., Rodríguez et al., 1994; Cleary et al., 2001). In-situ measurements of gravel barrier overwash sediment transport are very hard to obtain, and are potentially hazardous to people and equipment. Therefore, large-scale flume experiments can provide a valuable complement to field datasets. Although many laboratory experiments have been conducted of sediment transport in the swash or surf zone, only a handful of experiments on overwash have been conducted (Hancock and Kobayashi, 1994; Obhrai et al., 2008; Donnelly, 2008, Alessandro et al., 2010; Kobayashi et al., 2010; Park and Edge, 2010; Figlus et al., 2011), including the Barrier Dynamics Experiment (BARDEX) reported here (Williams et al., 2012). During BARDEX, overwash was simulated with waves that reached 1.0 m at breaking (Matias et al., 2012) and thus were significantly larger than those used in previous laboratory experiments, where wave heights were 0.14–0.33 m. Details about overwash thresholds based on the BARDEX experiment can be found in Matias et al. (2012).

In this work, the overwash simulations completed in Test Series E of the BARDEX experiment (Williams et al., 2012; Matias et al., 2012) are described. Results are presented from two perspectives: (1) the Eulerian perspective where overwash hydraulic variables and associated morphological changes are measured at the barrier crest, which represents the location that defines the transformation from swash to overwash; and (2) the Lagrangian perspective where high-intensity overwash flows and barrier properties are measured across the barrier. To collect data on overwash characteristics and bed changes, a large array of acoustic bed-level-sensors was deployed to collect bed/water surface elevation data at 4 Hz (cf., Turner et al., 2008). The obtained high-frequency data allowed overwash to be analysed on an event-by-event scale to provide valuable insight into overwash

100 behaviour over a gravel barrier. The primary objectives of this paper are to: (1)
101 provide a data-set of overwash hydraulics on gravel barriers; (2) improve and
102 develop empirical relations between key parameters of overwash flow; and (3)
103 gain insight about how overwash evolves across the backbarrier.

104

105 ## 2. EXPERIMENTAL SETUP AND METHODS

106 Experiments to study gravel barrier overwash were undertaken at proto-type scale
107 in the Delta Flume (The Netherlands) during the BARDEX project (Williams et al.,
108 2012). A gravel barrier (35 m long, 5 m wide and 4 m high) composed of sub-
109 rounded gravel ($D = 11$ mm) was constructed in the flume with the mid-barrier
110 crest located at a distance of 95 m from the wave paddle (Figure 1). The beach
111 profile used at the BARDEX experiment was loosely based on Slapton Sands,
112 Devon, England (Austin and Masselink, 2006).

113 Overwash was studied by exposing the barrier to variable wave and water-level
114 (h_s) conditions (Test Series E1 to E10; cf. Matias et al., 2012); however, for the
115 purpose of this study, only Test Series E10 will be considered because only during
116 this series did frequent backbarrier overwash occur. Test series E10 consisted of
117 eleven 15-min runs in which the water level ($h_s = 3.75$ m), peak wave period ($T_p =$
118 8 s), significant wave height ($H_s = 0.8$ m) and wave sequence were kept constant
119 to study the behaviour of the barrier under fully-developed overwash conditions.
120 All wave conditions conformed to a JONSWAP spectrum, specified by H_s and T_p.

121 Barrier morphology was surveyed before and after each run using a roller and
122 actuator which followed the bed profile from an overhead carriage (Figure 1d).
123 The sub-aerial barrier was monitored continuously at 4 Hz using acoustic bed-level

124 sensors (BLS) deployed at 0.5-m spacing (Figure 1e) and approximately 1 m above
125 the bed. These sensors are described in detail in Turner et al. (2008) and were also
126 used by Masselink and Turner (2012) to investigate swash dynamics during
127 BARDEX non-overwash runs. When mounted perpendicular to the bed, the sensors
128 use the time of flight of the reflected signal to obtain non-intrusive Eulerian
129 measurements, with an accuracy of c. 1 mm of the vertical distance to the closest
130 target: the sand level when the bed is "dry", and the water level when the bed is
131 submerged (Blenkinsopp et al., 2011). A more detailed analysis of BLS data was
132 undertaken for Test Series E10A, E10B and E10C because during those series full
133 overwash and significant deposition occurred on the sub-aerial back-barrier where
134 the BLS were located.

135 In this study, an overwash event is defined as a single passage of water above the
136 barrier crest; therefore, during the test runs a number of overwash events are
137 recorded at each BLS position. BLS records were pre-processed to separate
138 overwash events and bed-level events, which are measured by the variation in bed
139 elevation before and after the overwash event. For all BLS positioned landward of
140 the beach (BLS32 to BLS 44; Figure 1), every overwash event was identified and
141 isolated. For each overwash event, maximum and average depth, skewness of the
142 water depth distribution and duration of the event were computed.

143 Based on various morphologic and hydrodynamic parameters, Matias et al. (2012)
144 defined the Overwash Potential (*OP*, equation 1) as a parameter for quantifying the
145 likelihood of overwash, as well as providing an estimate of the overwash water
146 level relative to the barrier crest elevation:

147 $$OP = [1.1\ (0.35 \tan\beta\ (H_0L_0)^{0.5}+([H_0L_0(0.563(\tan\beta)^2+0.004)]^{0.5}/2))] + \eta - h_c$$

148 (1)

149 where $\tan\beta$ is beach slope, H_0 is offshore wave height, L_0 is the offshore wave
150 length, η is the sea level, including astronomical tides and storm surge, and h_c is the
151 barrier crest elevation. The first term of the equation (in square brackets) is the
152 2% exceedence for the vertical runup predicted by Stockdon et al. (2006). The
153 position and elevation of the barrier crest were determined at the end of the runs,
154 whereby the crest was defined as the location of the profile with the maximum
155 elevation. Beach slope was calculated for the barrier section between mean water
156 level and the top of the beach, where a break in slope was typically observed.

157 Overwash velocity was calculated following two methods: leading edge and
158 continuity. The leading edge velocity represents the velocity obtained using the
159 time delay between the leading edge of the overwash water between two BLS
160 positions. Because overwash leading edge velocities can be very fast (> 5 m s^{-1};
161 Matias et al., 2010) and the BLS sensors record at 4 Hz and are spaced at 0.5 m, the
162 leading edge of the overwash often arrives at two successive BLS positions at the
163 same time. Therefore, the leading edge velocity at the crest was computed between
164 BLS30 and BLS33 (before and after the crest position, 1.5 m apart; Figure 1) to
165 obtain an average value for the barrier crest area. The second methodological
166 adjustment is the use of the interpolated timing of water depth = 0.02 m. The
167 definition of 2 cm as the leading edge is somewhat arbitrary; however, this water
168 depth has been used in coastal engineering applications (e.g., Pullen et al., 2007).
169 Alternative measurements of the velocity close to the overwash leading edge were
170 obtained using the volume continuity method described in Blenkinsopp et al.

171 (2010). In brief, this technique computes a depth-averaged flow velocity based on
172 the local depth and the rate of change of flow volume landward of the point of
173 interest. Obtaining Eulerian estimates of the depth-averaged flow velocity
174 throughout the duration of each overwash event using continuity requires the
175 assumption that there is no infiltration into the bed. This assumption is clearly
176 invalid when considering a gravel barrier beach and as such the technique has only
177 been used to obtain initial flow velocities immediately after arrival of the overwash
178 leading edge when infiltration is expected to be limited.

179 The maximum distance across the barrier top and backbarrier that overwash
180 water reaches inland is here termed overwash intrusion, and was calculated for
181 every overwash event. Exact overwash intrusion is impossible to measure with
182 sensors at discrete locations, as intrusion is likely to be located somewhere
183 between two consecutive BLS. Therefore, intrusion was interpolated using the
184 overwash depth progression over the last two sensors. The distribution of
185 overwash intrusions is truncated by the backbarrier lagoon and the maximum
186 distance is 9.8 m.

187 Overwash discharge was computed for all overwash events using the average
188 depth and the depth-averaged velocity, derived using the continuity velocity
189 method, for each BLS position. The infiltration volume was computed by
190 subtracting the discharge volumes between two consecutive sensor positions.

191

192 ## 3. MORPHOLOGICAL DEVELOPMENT

193 During Test Series E10 the morphological changes of the cross-shore profile were
194 similar (Figure 1e). The beach was eroded and became flatter, while the barrier

195 elevation of the crest decreased and its position migrated lagoonward. The barrier
196 eroded on the seaward side and accreted on the lagoon side, and the steep rear-
197 side of the barrier was displaced lagoonward. Thus, during overwash the sediment
198 was eroded from the seaward side of the barrier, transported to the back-barrier
199 region and was deposited both in the sub-aerial and submerged part of the barrier
200 lagoon margin. These deposits created back-barrier slope instabilities which
201 periodically failed and avalanched down the submerged rear-side of the barrier
202 forming a steep prograding surface approximately parallel to the original slope.
203 This test demonstrated the importance of the lagoon water level in controlling the
204 geometry of the back-barrier deposit, particularly at the interception between the
205 subaerial backbarrier deposits and below the lagoon water level. The rate of
206 barrier lowering and widening was relatively constant (c. 7 mm min^{-1}) during Test
207 Series E10 (Figure 1e) and the average sediment transport rate across the barrier
208 crest was 0.1 $m^3m^{-1}min^{-1}$. The volume of sediment transported over the barrier
209 crest was similar for all runs (between 1.1 and 1.8 m^3m^{-1}, with an average of
210 1.3 $m^3 m^{-1}$). By the end of Test Series E10, the volume of the washover deposit had
211 increased by 13 $m^3 m^{-1}$. Approximately 68% of the washover sediment originated
212 from the beachface, with the remaining 32% coming from sediments in the crest
213 region that were deposited by overwash in the earlier test stages of Test Series
214 E10.

215 Despite hydrodynamic conditions being kept the same, overwash during Test
216 series E10 resulted in a progressive reduction of the barrier crest height, which in
217 turn, increased the likelihood of overwash. This can be summarized in a variation
218 of the Overwash Potential (OP, equation 1, Table 1) which is defined as the

219 difference between the runup elevation and the barrier crest elevation. At the
220 beginning of Test Series E10, OP = 0.75 m, but a decrease to 0.56 m was noticed on
221 the second run because of a significant reduction in beach slope (from 0.20 to 0.16,
222 Table 1), thus reducing the elevation of wave runup. This beach slope variation
223 acts as a negative feedback process by which the variation in beach slope retards
224 the occurrence of overwash. However, as the barrier crest height reduces, and the
225 beach slope compensation is insufficient, OP increases (from 0.56 m in E10B to
226 0.63 m in E10D to 0.71 m in E10G, Table 1). During Test Series E10, overwash
227 frequency progressively increased due to positive feedback, driven by barrier crest
228 lowering, until the barrier became permanently inundated and the experiment was
229 terminated. Although a corresponding increase in sediment transport would be
230 expected during barrier crest lowering, the rate of morphological change did not
231 increase (Figure 1e). This is attributed to increased dissipation of overwash flow
232 on the flatter back-barrier, promoting deposition, and a reduction in the beachface
233 gradient, enhancing wave dissipation at the front of the barrier.

234 During the latter runs of the E10 test series, the barrier crest was almost
235 continuously submerged and the backbarrier displaced lagoonward, in part
236 beyond the furthest BLS (BLS 45, Figure 1e). Therefore, a more detailed analysis of
237 overwash dynamics was only possible for the earlier runs, and only runs E10A,
238 E10B and E10C are discussed hereafter.

239

240 ## 4. OVERWASH OF THE CREST FROM AN EULERIAN PERSPECTIVE

241 ### *4.1. Overwash frequency and depth*

242 Figure 2 shows time series of overwash during runs E10A – E10C. Note that due to
243 the identical wave forcing for each of the test runs, the overwash sequence also
244 looks very similar (refer to the pause in overwash towards the end of the test
245 around 17:11). During runs E10A, E10B and E10C, 53, 53 and 62 overwash events
246 were measured, respectively. Therefore, mean overwash frequency was 0.06 Hz,
247 0.06 Hz and 0.07 Hz, for E10A, E10B and E10C, respectively, which corresponds to
248 a mean overwash period between 14 and 17 s. During Test Series E10 the waves
249 had a significant wave height of 0.8 m and peak period of 8 s; therefore,
250 approximately 50% of waves generated overwash flows. The average duration of
251 overwash events over the barrier crest was between 3.3 s and 3.5 s, with longer
252 overwash durations at the crest generally coinciding with the deeper flows .
253 Nevertheless, the longest overwash over the crest lasted for 6.75 s, but its
254 maximum water depth over the crest was only 26 cm. This was one of the few
255 situations were two swash events interacted to produce a single, double-peaked
256 overwash. Maximum overwash depth over the crest was 77 cm (Table 2), recorded
257 during E10C, while average overwash depth was only about 10 cm, for all runs.
258 Generally, overwash events are characterised by a peak in the water depth closely
259 following arrival of the leading edge, followed by a long shallow 'tail' (see
260 overwash 13 in Figure 3, as an example). The positive skewness of the overwash
261 depth distribution of 0.5 and 0.3 during runs E10A and E10B (Table 2) reflects this
262 shape. The more symmetrical overwash depth distributions during run E10C,
263 characterised by a skewness of only -0.04, is ascribed to the lower barrier crest
264 causing the overwash events to be more resemblant of propagating waves.

265 In the absence of field measurements, one way to infer overwash depth is through
266 the Overwash Potential (*OP*; Table 1). For runs E10A, E10B, and E10C, the

calculated values of *OP* were 0.75 m, 0.56 m, and 0.59 m, respectively. The same statistics were applied to overwash depth to compute the 2% exceedance overwash peak depth ($h_{2\%}$). For E10A, E10B, E10C h_2 was 0.60 m, 0.68 m, and 0.59 m, respectively. Although some non-systematic differences are noticed between *OP* estimates and depth measurements, the range of values is close (60-70 cm), which implies that *OP* can provide rough estimates of maximum overwash depth at the crest.

4.2. Overwash velocity

Overwash velocities over the crest were computed using both the continuity of flow volume method (referred to as 'continuity velocities') and the leading edge method (referred to as 'leading edge velocities'). Calculated velocities compare fairly well in general; however, maximum continuity velocity was 5 ms^{-1}, whereas leading edge velocity can have extremely high velocities that can attain up to 10 ms^{-1} (Figure 4). Mean continuity velocities are also smaller (2.6 ms^{-1}, 2.7 ms^{-1}, and 2.5 ms^{-1}, for E10A, E10B, and E10C, respectively) than mean leading edge velocities (3.0 ms^{-1}, 3.6 ms^{-1}, and 3.0 ms^{-1}, for E10A, E10B, and E10C, respectively). The average difference between the velocities computed with both methods is acceptable (0.5 ms^{-1}); however, individual differences can be much higher (>6 ms^{-1}; Figure 4). On the one hand, the leading edge method is more easily applicable as it can be applied using remote sensing techniques such as video; however, velocities as high as 10 ms^{-1} are only representative of the leading edge of the moving water, which is moving faster than the fluid behind it (as it has been considered for swash movement, e.g., Shen and Meyer, 1963). Accordingly, leading

edge velocities are not considered adequate for the computation of other variables such as overwash discharge and infiltration rate. The reason that these velocities are very different is related to the specific nature of water passage over the crest of steep beaches, which are similar to seawalls. For coastal engineering purposes, the way water overtops coastal structures is defined as either 'white water' or 'green water' (Pullen et al., 2007). In the 'green water' overtopping case there is a continuous sheet of water passing over the crest; in cases where the structures are vertical, the wave may impact against the wall and send a vertical plume of water against the crest (Pullen et al., 2007). In the case of gravel barriers, the beach slope is very steep and the visual observation of overtopping at the crest is such that the water is projected as a mixture of 'green water' and 'white water'. This was also observed in the field by Lorang (2002). Accordingly, the leading edge reaches several measurement points almost simultaneously, which results in extremely high leading edge velocities. However, the continuity method integrates the entire water column passing below each sensor, and therefore minimizes the 'white water' effect. Finally, one factor that should be taken into account is the equipment sampling frequency. This effect was somewhat minimized by methodological adjustments, but still the slow sampling rate may have contributed to some inaccuracy in this method.

BARDEX overwash average velocities at the crest were generally of the same order of magnitude as overwash velocity on sandy barriers (around 2 ms^{-1}) obtained from the literature regardless of the different methods used and the diverse geographical and oceanographic conditions. Leatherman (1977) obtained a mean overwash flow velocity of 1.95 ms^{-1} in Assateague Island (U.S.A.); Leatherman and Zaremba (1987) measured 0.5–2.0 ms^{-1} overwash flow velocities at Nauset Spit

316 (U.S.A.); a maximum of 1.5 ms^{-1} was the overwash flow through the Trabucador
317 Bar (Spain; Guillén et al., 1994); mean velocities of 2.0 ms^{-1} were obtained by
318 Holland et al. (1991) at the Isles Dernieres (U.S.A.); Bray and Carter (1992)
319 measured overwash flow velocities between 1 and 3 ms^{-1} at a barrier in Lake Erie
320 (U.S.A.).; and Matias et al. (2010) measured average velocities of 2.2–2.3 ms^{-1} for
321 non-storm overwash on Barreta Island (Portugal). As for experimental studies in
322 flumes, several overwash experiments have been undertaken (e.g., Hancock and
323 Kobayashi, 1994; Bradbury and Powell, 1992; Baldock et al., 2005; Alessandro et
324 al., 2010; Tinh et al., 2010), but published overwash velocities at crest are limited.
325 Srinivas et al. (1992) measured 0.8–1.2 ms^{-1} overwash velocity over a sandy
326 barrier; Schüttrumpf and Oumeraci (2005) measured up to 0.7 ms^{-1} overtopping
327 velocity over an impermeable dike; and Donnelly (2008) measured bore front
328 velocities smaller than 1.5 ms^{-1} on a sandy barrier. BARDEX maximum overwash
329 velocities (up to 5 ms^{-1} with continuity method and 10 ms^{-1} with leading edge
330 method) are significantly higher than those found in the literature for both
331 laboratory and field experiments. There have been measures of tsunami
332 inundation velocities reaching 8 to 11 ms^{-1} but those were from much deeper flows
333 (e.g. Matsutomi et al., 2010, Jaffe et al., 2011). The maximum leading edge velocity
334 measured by Holland et al. (1991) was 2.9 ms^{-1} whereas by Matias et al. (2010)
335 recorded velocities up to 5.7 ms^{-1}. There are a number of potential explanations for
336 this, including differences in the barrier geometry, wave and water level
337 conditions, methods of data collection and barrier sediments (i.e., sand versus
338 gravel). Probably one of the most important factors is the BARDEX beach
339 steepness and the narrowness of the barrier which promote the occurrence of very
340 energetic swash and overwash.

About 95% of all overwash events measured during the BARDEX experiment (168 events) were supercritical flows with average Froude number of 2. These data also showed that there is a relation between leading edge velocity and depth at crest (Figure 5). This relation can be described in two forms: analytical and empirical. The analytical form uses a classical dam break equation, which has also been used for the tip of bores in the swash zone (e.g., Jiang et al., 2010):

$$u_{crest} = 2\ (g\ h_c)^{0.5} \quad (2)$$

Where u_{crest} is the overwash leading edge velocity (m s^{-1}), g is acceleration due to gravity (m s^{-2}) and h_c is the overwash water depth (m). Additionally, empirical forms of equation 2 based on laboratory or field data are available. For example, Holland et al. (1991) used field data from video to obtain an empirical expression to relate overwash depth and velocity:

$$u_{crest} = 2.6\ (g\ h_c)^{0.5} \quad (3)$$

A similar result was obtained by Donnelly (2008) using laboratory and field data (including Holland et al., 1991):

$$u_{crest} = 1.53\ (g\ h_c)^{0.5} \quad (4)$$

The same type of power fitting model was applied to BARDEX data, and a relation was obtained (Figure 5a):

$$u_{crest} = 2.35\ (g\ h_c)^{0.5} \quad (5)$$

The curve adjustment using equation 5 had $R^2 = 0.52$ and RMSE = 1.32 ms^{-1}. The constant of proportionality varies between the equations, with the coefficient obtained using BARDEX data (2.35; equation 5) comparable to the result of Holland et al. (2.6; equation 3) and the analytical approach (2; equation 2). The

same approach was used to analyse the relation between depth and velocity, but using the velocity obtained with the continuity method (Figure 5b). The obtained coefficient was smaller (1.86), closer to the one obtained by Donnelly (1.53; equation 4). It should be pointed out that differences between coefficients are expected as BARDEX experimental data covers a wider range of overwash leading edge velocities (Figure 5) than other data-sets, but overwash depths were always shallower than 0.8 m (Figure 2).

4.3. Overwash discharge

For the computation of overwash discharge over the crest, the depth-averaged velocities (continuity velocities) were deemed more suitable, as explained previously. The majority of individual overwash discharges recorded in all runs were < 2 $m^3 m^{-1}$, but maximum individual overwash discharge was about 6 $m^3 m^{-1}$ (Figure 6). The average individual discharge rate computed over the duration of the 15-min test runs was very similar for all three runs: 0.31 $m^3 m^{-1} s^{-1}$, 0.35 $m^3 m^{-1} s^{-1}$ and 0.31 $m^3 m^{-1} s^{-1}$. Overall, the total overwash discharge into the lagoon during the 15-min runs E10A, E10B and E10C was 55 $m^3 m^{-1}$, 62 $m^3 m^{-1}$ and 67 $m^3 m^{-1}$, respectively. The increased discharge from E10A to E10C is in line with the increase in overwash potential related to crest lowering discussed previously, and an associated increase in total overwash duration from 177 seconds of overwash over the barrier crest in E10A to 215 seconds in E10C.

BARDEX overwash discharges over the barrier crest are high when compared to safety standards for coastal engineering structures (e.g., Pullen et al., 2007). With overtopping/overwash water discharge over the crest of a structure/barrier

388 higher than 0.05 $m^3 m^{-1} s^{-1}$ or a single overtop volume of water higher than 1 $m^3 m^{-1}$, no pedestrians or vehicles would safely pass behind the barrier, even at low speed. A relatively low wave energy was simulated during Test Series E10 of BARDEX experiment ($H_s = 0.8$ m), when compared with wave energy during overwash of gravel barriers, when storm wave height may be 3.5 m (Hurst Spit, U.K., Bradbury and Powell, 1992), 3.5 m (Carnsore, Ireland, Orford and Carter, 1984), 4 m (Rialto Beach, U.S.A., McKay and Terich, 1992), 4 m (Slapton Sands, U.K., Alegria-Arzaburu and Masselink, 2010), 5 m (Porlock Barrier, U.K., Orford et al., 2003), 6.5 m (Chesil Beach, U.K., May and Hansom, 2003). Assuming that equations 2 to 5 are valid approaches, then overwash velocity at crest is solely dependent on the overwash depth, and therefore *OP* at the crest. In nature, barrier crest elevation is defined by the distribution of wave runup as a function of breaker height, beach slope and bed roughness (Orford et al., 2002). Barrier elevation also reflects a balance between runup sufficient to deposit material at the beach crest (overtop) and runup sufficient to exceed the crest and move sediments onto the backbarrier slope (overwash). The combination that is required to produce positive values of *OP* is therefore site-specific, requiring either a low-lying barrier with moderate wave energy at one end of the scale, or a high-elevation barrier during extreme storms, at the other. For both situations, individual overwash discharges may be similar to the ones measured during the BARDEX experiments given that *OP* values are similar. However, overwash frequency during the event may be different as it is also related to wave period, and therefore the total volume of water that passes the barrier crest during the whole overwash event may vary greatly.

412

5. OVERWASH FROM A LAGRANGIAN PERSPECTIVE

5.1. Overwash depth across the barrier

Overwash depth across the barrier varied significantly, both within each overwash event and from one event to another. Maximum depths were recorded at the barrier crest, but the depth decrease across the backbarrier varied from event to event. As an example, Figure 3 shows overwash events 12, 13 and 14 at the backbarrier, during E10B. The three events had similar durations over the crest, (4.00 s to 4.25 s), but event 13 was clearly the largest, with 46 cm water depth at the crest. Events 12 and 14 had depths of 19 cm and 18 cm at the crest, respectively. Event 12 reached the lagoon, but event 14 did not. Overwash velocities at the crest for events 12 and 14 were 3.2 m s^{-1} and 3.0 m s^{-1}, respectively. Therefore, the overwash progression at the backbarrier is sensitive to small variations in the combination of hydrodynamic and morphological factors at the crest. This includes variations in sediment properties across the backbarrier that influence the infiltration rate, and therefore the progression into the lagoon.

Considering all overwash events from the three runs (E10A, B and C), the peak average depth over the crest is 21 cm, at the backbarrier slope break is 12 cm, and at the steep slope, before the lagoon, is 9 cm. To gain a more integrated perspective of the overwash at the backbarrier, an average overwash peak depth profile was produced (Figure 7a). Only overwash events that reach the lagoon were used for this profile, so that there is a depth record for all sensors. Overwash flow across the barrier can be divided into 3 sections: at the crest, barrier top and backbarrier steep slope. At the barrier crest there is a sudden 50% decrease in flow depth (37

437 cm to 19 cm) within the first 1 m (see also Figure 3, event 13) as the flow
438 progresses over the back of the crest and infiltrates into the bed. Over the first 3 m
439 of the barrier top (from $x = 94$ m to 97 m, Figure 7a), mean overwash depth
440 decreases to 12 cm, but across the whole steep backbarrier slope the water depth
441 profile is almost parallel to the barrier profile, with a depth of approximately 10
442 cm (Figure 7a).

443 The average overwash flow across the barrier at BARDEX is different from water
444 progression schemes used for overtopping and overwash modelling as shown in
445 Figure 7b (e.g., Schuttrumpf and Oumeraci, 2005). In these simplifications only
446 two sections are generally identified (Schuttrumpf and Oumeraci, 2005; Pullen et
447 al., 2007) and sometimes only one (Nguyen et al., 2006). In these simplified
448 geometric shapes there is no such sharp decrease in flow depth at the crest and
449 also there is a steady depth decrease across the backbarrier.

450 In the case of overtopping of coastal structures, where the profile is artificially
451 built and the bed is impermeable or consists of large blocks, the overwash profile
452 is different from that recorded during BARDEX. Even in the case of natural gravel
453 barriers, there is a variety of profile morphologies, dimensions, wave exposure, etc.
454 The beach profile used at the BARDEX experiment was based on Slapton Sands,
455 Devon, England (Austin and Masselink, 2006). Many gravel barriers are also
456 narrow with a steep backbarrier (Figure 8), such as Dunwich-Walberswick barrier,
457 Suffolk coast, U.K. (Pye and Blott, 2009) or Miseners Long Beach, Nova Scotia,
458 Canada (Taylor et al., 1997), but others are wider and flatter such as Tacumshin
459 barrier, southeast coast, Ireland (Orford et al., 1988). The average overwash
460 profile measured during BARDEX is not representative of all overwash hydraulic

characteristics of all gravel barriers, but it is probably closer to real situations than the simplified schemes from the coastal engineering literature. Probably, wider gravel barriers would have even more or different overwash sections than those identified in the BARDEX case, for example pouding in small depressions, or alongshore-directed flow sections induced by irregularities and obstacles on the barrier top morphology.

5.2. Overwash intrusion

The intrusion distance of overwash events beyond the barrier crest was variable between 0.5 m and 9.8 m, when it reached the lagoon water. The longest overwash events were those with greater depths over the crest; conversely, limited intrusion overwash reaches the crest with shallow depths (Figure 9). Discounting those events which reached the lagoon there is a linear relation between overwash depth at the crest and the intrusion distance (Figure 9). The relation is expressed by:

$$h_c = 0.03\, i \qquad (6)$$

where h_c = water depth at the crest and i = intrusion distance in relation to crest. The adjustment expressed in equation 6 has a $R^2 = 0.65$ and a RMSE = 0.05 m, and does not use data from events which reached the lagoon when the intrusion distance > 9.8 m. This relation is useful for coastal management since it provides an estimate of where the overwash may reach inland, and therefore the likely hazard areas. Note that this relation assumes a backbarrier without obstacles, depressions (wet or dry), etc, and is probably sensitive to morphology and sediment grain-size and packing variations. As mentioned earlier, the gravel

484 barrier shape is variable (Figure 8) which influences the intrusion. The distance to
485 the lagoon is certainly one of the most important limiting factors, but also the
486 backbarrier slope, the width of the barrier top, the barrier grain-size and sorting,
487 and the degree of saturation or depth to water table. The influence of these and
488 other variables cannot be determined solely with data from the BARDEX
489 experiment. Future research efforts should focus on providing complimentary data
490 on different barriers.

491 Intrusion is one of the most important parameters for coastal zone management,
492 particularly in locations with human development on the coast. The safety
493 standards on the coast curtail urban development to beyond maximum overwash
494 intrusion distance for storm conditions of a given return period. Therefore, the
495 availability of a simple and reliable intrusion predictor is significant. Management
496 plans often rely on simple predictive tools rather than sophisticated methods, and
497 the relation obtained here may move us a step further in this research.

498

499 ### *5.3. Overwash infiltration*

500 An assessment of the volume of water infiltrating into the back-barrier was
501 obtained by computing the flow volume passing BLS 32 to 45 (Figure 1) during
502 each overwash event, and assuming that any difference in flow volume between
503 adjacent sensors must have been lost due to infiltration into the barrier. Figure 10
504 shows the variation of the total overwash volume per event with cross-shore
505 location on the back-barrier for the 53 overwash events observed during run
506 E10B. It is observed that for all events, the measured volume decreases in an

507 approximately linear manner with distance landward of the barrier crest. This
508 observation implies that the rate of volume loss within each event is
509 approximately constant as the overwash flows propagate over the back-barrier,
510 though there is some evidence that the rate of volume loss decreases slightly with
511 the flow depth. Assuming a constant rate of volume loss during each event, but a
512 different rate between different events, Figure 11 displays the mean flow volume
513 lost through the barrier during each overwash event per metre length of back-
514 barrier as a function of the peak overwash depth at the barrier crest (BLS32). It is
515 observed that between 0.046 and 0.865 $m^3 m^{-1}$ width of flow volume is lost per
516 metre of barrier and the volume lost increases strongly with increasing overwash
517 depth. This result is explained by the fact that infiltration rates into the barrier
518 will increase as the head of water increases.

519

520 ## 5.4. Overwash-induced bed changes across the barrier

521 Using data from bed-level sensors (BLS), an event-by-event analysis of local bed
522 level changes is possible. It is acknowledged that sediment flux per event is a more
523 appropriate measure of sediment transport per overwash (Blenkinsopp et al.,
524 2011); however, as overwash events cause sediment to be transported into the
525 lagoon where it cannot be measured by the BLS, such estimates were not possible.
526 There are three main areas of sub-aerial barrier changes due to overwash, each
527 represented in the following description by changes recorded by particular bed-
528 level sensors: the crest (BLS 32; Figure 1), the barrier top (BLS 38) and the
529 backbarrier region before the lagoon (BLS 42). Figure 12a shows the cumulative
530 bed-level variation throughout E10A until E10C for the three selected locations. As

mentioned, BLS32 and BLS38 sites experienced net erosion (26 cm and 14 cm, respectively) and BLS 42 experienced net accretion (11 cm) and was also characterised by the largest individual bed level changes (Figure 12b). However, it is noted that the bed variations induced by the overwash flows were not always in the same direction for each site; rather, a high number of very small positive or negative bed changes were recorded, mostly in the range ± 2 cm (Figure 12b). These positive (accretion) and negative (erosion) changes tended to almost balance out over the duration of each test leading to extremely small average bed changes per overwash event given the roughness of gravel bed: -1.6 mm, -1.5 mm, and 1.9 mm, respectively for BLS32, BLS38, and BLS42. Surprisingly, the landward site (BLS42) recorded the highest positive and negative changes per event, despite the fact that overwash flow velocities were smallest at this location (Figure 12d). According to data presented in this study, there is no apparent direct relationship between the overwash flow velocity and the magnitude of local morphological change (Figure 12c). Overall erosion at BLS32 and BLS38 occurred due to a slightly higher number of erosive than accretionary events (Figure 12b). For the three analysed cross-shore locations, the average positive and negative bed level changes were almost equal, i.e. for BLS32 the average accretionary overwash promoted an 8 mm bed raise while the average erosive overwash promoted an 8 mm bed lowering. For BLS 38, average accretion and erosion were 7 mm and 8 mm, respectively; and for BLS42, average accretion and erosion were 20 mm and 25 mm respectively. Therefore, the overall morphological variation at each location is mostly dependent on the number of events that promote erosion/accretion. For BLS32 and BLS38, 57% of events promoted erosion leading

555 to an overall lowering of the bed at these locations, whereas for BLS42, 59% of
556 events caused increases in bed elevation leading to net accretion.

557 Results from the event-by-event analysis reveal that net morphological changes
558 result from slight variations in the proportion of accretionary and erosive events,
559 since mean changes per event are very similar. This is probably because at the
560 barrier top (where sensors 32 to 42 are located, Figure 1) the sediments are in a
561 section of their total transport path from the beach to the distal backbarrier. For
562 each overwash event, there is an almost even balance of sediments arriving and
563 leaving that position, i.e. at each location the amount of sediment arriving due to
564 the incoming flow is only slightly different from the amount of sediment leaving
565 due to the outgoing flow. Figure 1e indicates how regular this process is, with
566 similar total changes over the barrier as a whole occurring during each of runs
567 E10A, E10B and E10C. It is suggested that the more energetic overwash flows
568 transport a relatively large amount of sediment to each location, but
569 simultaneously erode more sediment from that site, and vice-versa, indicating why
570 bed changes appear to be independent from overwash velocity.

571 From the results presented here, it seems that prediction of bed changes at each
572 location cannot be done in a deterministic way, since similar flows promote
573 different bed variations. Rather, the overall morphological variation result from a
574 slight imbalance balance between the percentages of erosive/accretionary events,
575 i.e. net accretion/erosion occurs when more than 50% of overwash flows induce
576 erosive/accretionary bed changes. Therefore, an important factor to predict
577 morphological changes is the correct location of the nodal point, seaward of which
578 flows have an erosive balance and landward of each more than 50% of flows

induce accretion. For the BARDEX barrier, the nodal point is located around BLS40, a significant distance (5–7 m) landward of the barrier crest (Figure 1e). This distance corresponds to the location of the average overwash flow intrusion distance for all runs analysed here (6 m from the barrier crest; Figure 9). Average intrusion can be determined from equation 6, given the average depth over the crest, which can be measured or predicted by the computation of the overwash potential (*OP*, equation 1 of section 3).

6. CONCLUSIONS

The paper provides the first measurements of hydrodynamic and morphological evolution of a gravel barrier during overwash at proto-type scale. The observed morphological evolution of the barrier reveals a net erosion of the beach and barrier crest, with sediments transported to the back-barrier region and deposited both in the sub-aerial and submerged part of the barrier lagoon margin. An event-by-event analysis of bed changes shows that the barrier top is part of an onshore transport path under intermittent and variable overwash flows that either erode/accrete sediments on their way to the steep backbarrier slope that is mostly accreting.

It is observed that from test Series E10A to E10C, the overwash frequency increases, maximum overwash depth increases (with approximately 50% of waves generating overwash flows), and depth curves become more symmetrical resembling propagating waves. Mean overwash velocities at the barrier crest were relatively high (around 3 m s^{-1}) as well as the total overwash discharge into the lagoon. Considering safety standards for coastal engineering structures, these

603 overwash volumes would imply that no pedestrians or vehicles would safely pass
604 behind the barrier, even with relatively low wave energy simulated during
605 BARDEX ($H_s = 0.8$ m).

606 According to data collected during this study, overwash flow across the barrier can
607 be divided into 3 sections: at the crest (where overwash flow depth show a sudden
608 decrease), barrier top (with a smaller reduction in overwash depth) and
609 backbarrier steep slope (where the depth is relatively constant). This depth profile
610 is different from water progression schemes used for overtopping and overwash
611 modelling.

612 Two relations are obtained: one that relates peak overwash depth at the barrier
613 crest to velocity at the crest (power fit model); and another that relates peak
614 overwash depth to intrusion distance (linear fit model). It must be stressed that
615 the relations identified in this study are empirical and developed based on
616 laboratory conditions. Nevertheless, relations based on results from flume
617 experiments have been proven to have valuable contributions for real situations,
618 for example, the runup equation of Hunt (1959), and the coarse grained profile
619 model detailed by Van der Meer (1988). Data from other experiments, and most
620 importantly from fieldwork are essential to verify the range of applicability of
621 these relations, perhaps augmented by numerical modelling. A lack of published
622 data on the hydraulics of overwash over gravel barriers does not allow such an
623 evaluation to be done within this study.

624 Results presented in this study provide a valuable insight of overwash on gravel
625 barriers and a detail analysis of processes in an event-by-event scale. Results
626 should be used with care since field and laboratory situations are different;

however, given the technical difficulty and hazard of undertaking fieldwork during overwash in gravel barriers, the obtained datasets are unique and useful to improve models of barrier overwash and breaching.

Acknowledgements

The data reported here were collected in the Delta flume (The Netherlands) as part of the EU-funded BARDEX project (HYDRALAB III Contract no. 022441 (RII3), Barrier Dynamics Experiment). Ana Matias was supported by the RUSH Project (From Runup to Overwash, reference PTDC/CTE-GIX/116814/2010) and Gerd Masselink was supported by the NUPSIG project (New Understanding and Prediction of Storm Impacts on Gravel Beaches) funded by the EPSRC (reference EP/H040056/1) We would like to thank all BARDEX collaborators for their contributions, but in particular those who participated in overwash experiments: Celia Swinkels, Daniel Buscombe, Rita Carrasco, Amaia Alegria-Arzaburu, and Saul Reynolds.

References

Alegria-Arzaburu, A. R., and Masselink, G. (2010). Storm response and beach rotation on a gravel beach, Slapton Sands, U.K. Marine Geology 278, 77-99.

Alessandro, F., Fortes, C. J., Ilic, S., James, M., Sancho, F., Schüttrumpf, H., and Tomasicchio, G. R. (2010). Wave storm induced erosion and overwash in large-scale flume experiments. Proceedings of the HYDRALAB III Joint User Meeting. Hannover, Germany.

650 Austin, M. J., and Masselink, G. (2006). Observations of morphological change and
651 sediment transport on a steep gravel beach. Marine Geology 229, 59-77.
652 Baldock, T. E., Hughes, M. G., Day, K., and Louys, J. (2005). Swash overtopping and
653 sediment overwash on a truncated beach. Coastal Engineering 52, 633-645.
654 Blenkinsopp, C., Turner, I., Masselink, G., and Russel, P. (2010). Validation of
655 volume continuity method for estimation of cross-shore swash flow velocity.
656 Coastal Engineering 57, 953-958.
657 Blenkinsopp, C., Turner, I., Masselink, G., and Russel, P. (2011). Swash zone
658 sediment fluxes: field observations. Coastal Engineering 58, 28-44.
659 Bradbury, A., Cope, S. N., and Prouty, D. B. (2005). Predicting the response of
660 shingle barrier beaches under extreme wave and water level conditions in
661 Southern England. Proceedings of Coastal Dynamics, ASCE, Barcelona, Spain.
662 Bradbury, A. P., and Powell, K. A. (1992). The short term profile response of shingle
663 spits to storm wave action. Proceedings of International Conference on
664 Coastal Engineering, Venice, Italy, pp. 2694-2707.
665 Bray, M. J., and Duane, W. (2001). Porlock Bay: geomorphological investigation and
666 monitoring - gravel barrier breaching and tidal lagoon development.
667 Environment Agency Science Report SC980010/SR, pp. 111.
668 Bray, T. F., and Carter, C. H. (1992). Physical processes and sedimentary record of a
669 modern, transgressive, lacustrine barrier island. Marine Geology 105, 155-
670 168.
671 Buscombe, D., and Masselink, G. (2006). Concepts in gravel beach dynamics. Earth-
672 Science Reviews 79, 33-52.

673 Carter, R. W. G., and Orford, J. D. (1993). The morphodynamics of coarse clastic
674 beaches and barriers: a short term and long term perspective. Journal of
675 Coastal Research SI 15, 158-179.

676 Cleary, W. J., McLeod, M. A., Rauscher, M. A., Johnston, M. K., and Riggs, S. R. (2001).
677 Beach nourishment on hurricane impacted barriers in Southeastern North
678 Carolina, USA: Targeting shoreface and tidal inlets sand resources. Journal of
679 Coastal Research SI 34, 232-255.

680 Donnelly, C. (2008). Coastal overwash: processes and modelling. Lund University,
681 Sweden, 53 pp + papers.

682 Figlus, J., Kobayashi, N., Gralher, C., and Iranzo, V. (2011). Wave overtopping and
683 overwash of dunes. Journal of Waterway, Port, Coastal, and Ocean
684 Engineering, 137, 26-33.

685 Fritz, H.M., Phillips, D.A., Okayasu, A., Shimozono, T., Liu, H., Mohammed, F.,
686 Skanavis, V., Synolakis, C.E., Takahashi, T. (2012). The 2011 Japan tsunami
687 current velocity measurements from survivor videos at Kesennuma Bay
688 using LiDAR. Geophysical Research Letters, 39, L00G23.

689 Guillén, J., Camp, J., and Palanques, A. (1994). Short-time evolution of a microtidal
690 barrier - lagoon system affected by storm and overwashing: the Trabucador
691 Bar (Ebro Delta, NW Mediterranean). Zeitschrift fur Geomorphologie 38,
692 267-281.

693 Hancock, M. W., and Kobayashi, N. (1994). Wave overtopping and sediment
694 transport over dunes. Proceedings of 24th Conference on Coastal
695 Engineering, ASCE, Kobe, Japan, pp. 2028-2042.

Hart, D. E. (2007). River mouth lagoon dynamics on mixed sand and gravel barrier coasts. Journal of Coastal Research, 927-931.

Holland, K. T., Holman, R. A., and Sallenger, A. H. (1991). Estimation of overwash bore velocities using video techniques. Proceedings of Coastal Sediments '91, USACE, Seattle, Washington, USA., pp. 489-497.

Hunt, I.A. (1959). Design of seawalls and breakwaters. Journal of the Waterways and Harbors, Division 85(WW3), 123-152.

Jaffe, B., Buckley, M., Richmond, B., Strotz, L., Etienne, S., Clark, K., Watt, S., Gelfenbaum, G., Goff, J. (2011). Flow speed estimated by inverse modelling of sandy sediment deposited by the 29 September 2009 tsunami near Satitoa, east Upolu, Samoa. Earth-Science Reviews, 107, 23-37.

Jiang, A. W., Hughes, M., Cowell, P., Gordon, A., Savioli, J. C., and Ranasinghe, R. (2010). A hybrid model of swash-zone longshore sediment transport on reflective beaches. Proceedings of International Conference on Coastal engineering, Shanghai, China.

Kobayashi, N., Farhadzadeh, A., Melby, J., Johnson, B., and Gravens, M. (2010). Wave overtopping of levees and overwash of dunes. Journal of Coastal Research, 26(5), 888-900.

Leatherman, S. P. (1977). Overwash hydraulics and sediment transport. Proceedings of Coastal Sediments '77, ASCE, Charleston, USA, pp. 135-148.

Leatherman, S. P., and Zaremba, R. E. (1987). Overwash and aeolian processes on a U.S. Northeast coast barrier. Sedimentary Geology 52, 183-206.

718 Lorang, M. S. (2002). Predicting the crest height of a gravel beach. Geomorphology
719 48, 87-101.

720 Masselink, G and Turner, I.L. (2012). Large-scale laboratory investigation into the
721 effect of varying back-barrier lagoon water levels on gravel beach
722 morphology and swash zone sediment transport. . Coastal Engineering, 63,
723 23-38.

724 Matias, A., Ferreira, Ó., Vila-Concejo, A., Morris, B., and Dias, J. A. (2010). Short-term
725 morphodynamics of non-storm overwash. Marine Geology 274, 69-84.

726 Matias, A., Williams, J. J., Masselink, G., and Ferreira, Ó. (2012). Overwash threshold
727 for gravel barriers. Coastal Engineering 63, 48-61.

728 Matsutomi, H., Okamoto, K., and Harada, K. (2010). Inundation flow velocity of
729 tsunami on land and its practical use. Proceedings of International
730 Conference on Coastal engineering, Shanghai, China.May, V.J. and Hansom,
731 J.D. (2003). Coastal Geomorphology of Great Britain. Geological Conservation
732 Review Series, No. 28, Joint Nature Conservation Comittee, Peterborough,
733 754 pp.

734 McKay, P. J., and Terich, T. A. (1992). Gravel barrier morphology: Olympic National
735 Park, Washington State, USA. Journal of Coastal Research 8, 813-829.

736 Nguyen, X. T., Donnelly, C., and Larson, M. (2006). A new empirical formula for
737 coastal overwash volume. Proceedings of Vietnam-Japan Estuary Workshop
738 2006, Hanoi, Vietnam, pp. 60-65.

739 Obhrai, C., Powell, K., and Bradbury, A. (2008). A laboratory study of overtopping
740 and breaching of shingle barrier beaches. Proceedings of International
741 Conference on Coastal Engineering, Hannover, Germany, pp. 1497-1508.

742 Orford, J., and Carter, R. W. G. (1984). Mechanisms to account for the longshore
743 spacing of overwash throats on a coarse clastic barrier in southeast Ireland.
744 Marine Geology 56, 207-226.

745 Orford, J. D., and Carter, R. W. G. (1982). Crestal overtop and washover
746 sedimentation on a fringing sandy gravel barrier coast, Carnsore Point,
747 Southeast Ireland. Journal of Sedimentary Petrology 52, 265-278.

748 Orford, J. D., Carter, R. W. G., Forbes, D. L., and Taylor, R. B. (1988). Overwash
749 occurrence consequent on morphodynamic changes following lagoon outlet
750 closure on a coarse clastic barrier. Earth Surface Processes and Landforms
751 13, 27-35.

752 Orford, J. D., Carter, R. W. G., Jennings, S. C., and Hinton, A. C. (1995). Processes and
753 timescales by which a coastal gravel-dominated barrier responds
754 geomorphologically to sea-level rise: Story Head Barrier, Nova Scotia. Earth
755 Surface Processes and Landforms 20, 21-37.

756 Orford, J. D., Cooper, J. A. G., Jackson, D., Malvarez, G., and White, D. (1999). Extreme
757 storms and thresholds on foredune stripping at Inch Spit, South-West
758 Ireland. Proceedings of Coastal Sediments '99, New York, USA, pp. 1852-
759 1866.

760 Orford, J. D., Forbes, D. L., and Jennings, S. C. (2002). Organisational controls,
761 typologies and time scales of paraglacial gravel-dominated coastal systems.
762 Geomorphology 48, 51-85.

763 Orford, J., Jennings, S., and Pethick, J. (2003). Extreme storm effect on gravel-
764 dominated barriers. Proceedings of Coastal Sediments '03, Florida, USA,
765 ASCE, CD-ROM.

766 Park, Y. H., and Edge, B. L. (2010). An empirical model to estimate overwash.
767 Journal of Coastal Reseach 26, 1157-1167.

768 Pullen, T., Allsop, N. W. H., Bruce, T., Kortenhaus, A., Schuttrumpf, H., and Van der
769 Meer, J. W. (2007). Wave overtopping of sea defences and related structures:
770 assessment manual. EurOtop. Die Küste, 73. 178 pp.

771 Pye, K., and Blott, S. J. (2009). Progressive breakdown of gravel-dominated coastal
772 barrier, Dunwich-Walberswick, Suffolk, U.K.: processes and implications.
773 Journal of Coastal Reseach 25, 589-602.

774 Rodríguez, R. W., Webb, R. M. T., and Bush, D. M. (1994). Another look at the impact
775 of Hurricane Hugo on the shelf and coastal resources of Puerto Rico, USA.
776 Journal of Coastal Research 10, 278-296.

777 Schüttrumpf, H., and Oumeraci, H. (2005). Layer thicknesses and velocities of wave
778 overtopping flow at seadikes. Coastal Engineering 52, 473-495.

779 Shen, M. C., and Meyer, R. E. (1963). Climb of a bore on a beach. Part 3. Runup.
780 Journal of Fluid Mechanics 16, 113-125.

781 Srinivas, R., Dean, R. G., and Parchure, T. M. (1992). Barrier island erosion and
782 overwash study - Volume 1. Coastal and Ocean Engineering Department,
783 University of Florida, 92 pp.

784 Stockdon, H.F., Holman, R.A., Howd, P.A., Sallenger, A.H., 2006. Empirical
785 parameterization of setup, swash, and runup. Coastal Engineering, 53, 573-
786 588.

787 Stone, G., Liu, B., Pepper, D. A., and Wang, P. (2004). The importance of
788 extratropical and tropical cyclones on the short-term evolution of barrier
789 islands along the northern Gulf of Mexico, USA. Marine Geology 210, 63-78.

790 Taylor, R. B., Forbes, D. L., Frobel, D., Shaw, J., and Parkes, G. (1997). Hurricane
791 Hortense strikes Atlantic Nova Scotia: An examination of beach response and
792 recovery. Geological Survey of Canada, Open File 3503.

793 Tinh, N. X., Larson, M., Donnelly, C., and Tanaka, H. (2010). Laboratory experiment
794 on cross-shore barrier spit evolution by storm dynamics. Proceedings of
795 International Conference on Coastal Engineering 2010, ASCE, Shanghai,
796 China.

797 Turner, I. L., Russell, P. E., and Butt, T. (2008). Measurement of wave-by-wave bed-
798 levels in the swash zone. Coastal Engineering 55, 1237-1242.

799 Van der Meer, J. (1988). Rock slopes and gravel beaches under wave attack. Delft
800 Hydraulics Publications, vol. 396.

801 Williams, J. J., Buscombe, D., Masselink, G., Turner, I. L., and Swinkels, C. (2012).
802 Barrier dynamics experiment (BARDEX): Aims, design and procedures.
803 Coastal Engineering 63, 3-12.

804

Figure captions

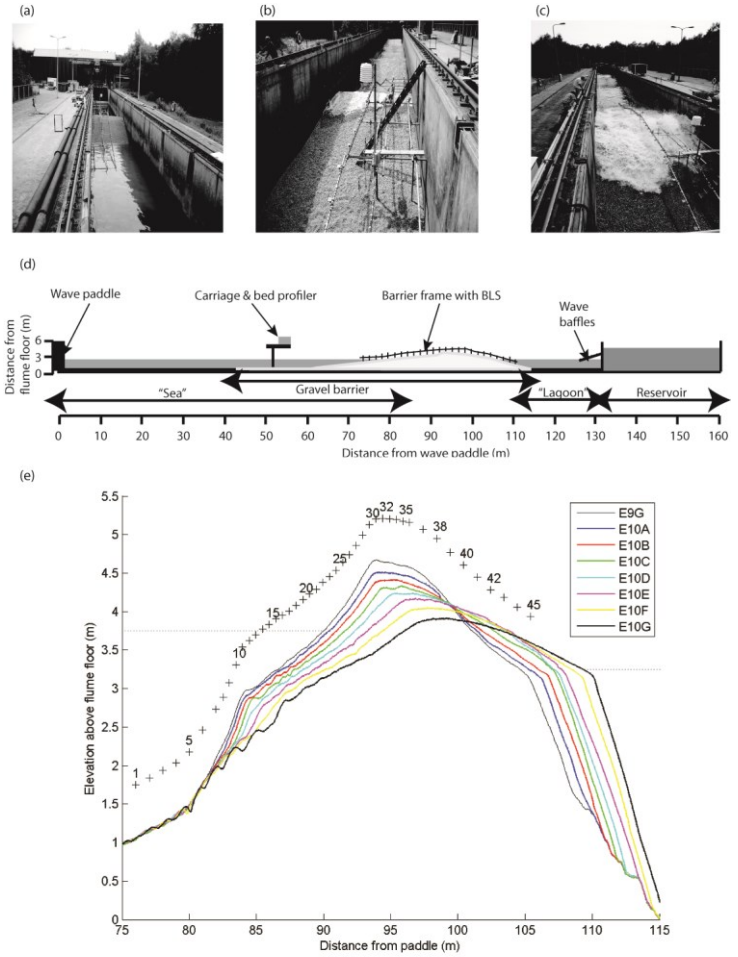

Figure 1. (a) View of the barrier towards the lagoon; (b) View towards the paddle of barrier overtopping; (c) View towards the paddle of barrier overwash; (d) Sketch of the experiment cross-section within the Delta flume; (e) Barrier cross-shore profiles from Test Series , E10A to E10G. Crosses on top of the profiles represent the BLS location and number identification. Water level on the 'sea' side (paddle side, to the left) and 'lagoon' side are also represented in dash-lines.

814

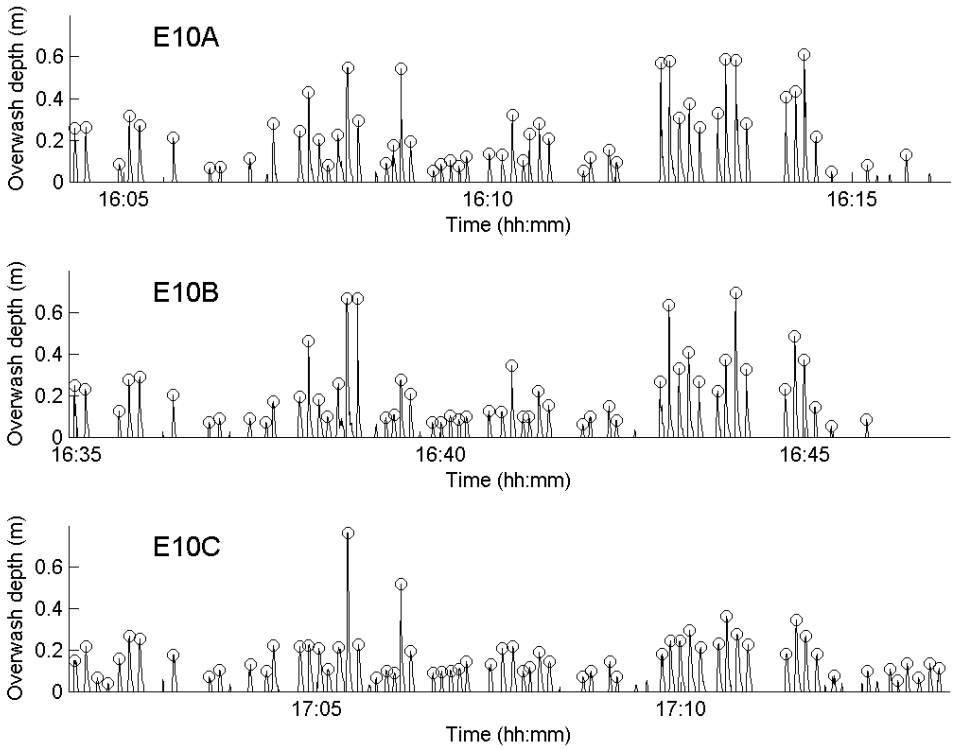

815

816 Figure 2. Time-series of extracted overwash depth data recorded during Test

817 Series E10A, E10B and E10C, with the peak depth of each overwash event marked

818 with a circle.

819

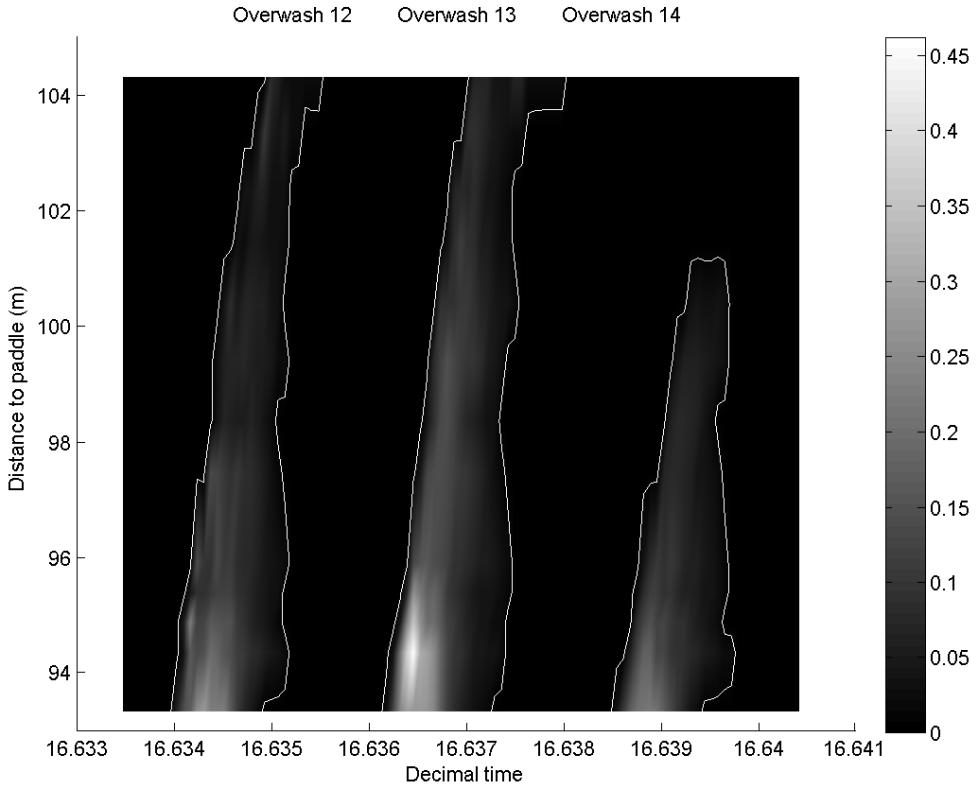

820

821 Figure 3. (a) Time-series of the overwash depth over time (xx axis) and across the
822 barrier (yy, lagoon is upwards) for three overwash events (12, 13 and 14, of Test
823 Series E10B).

824

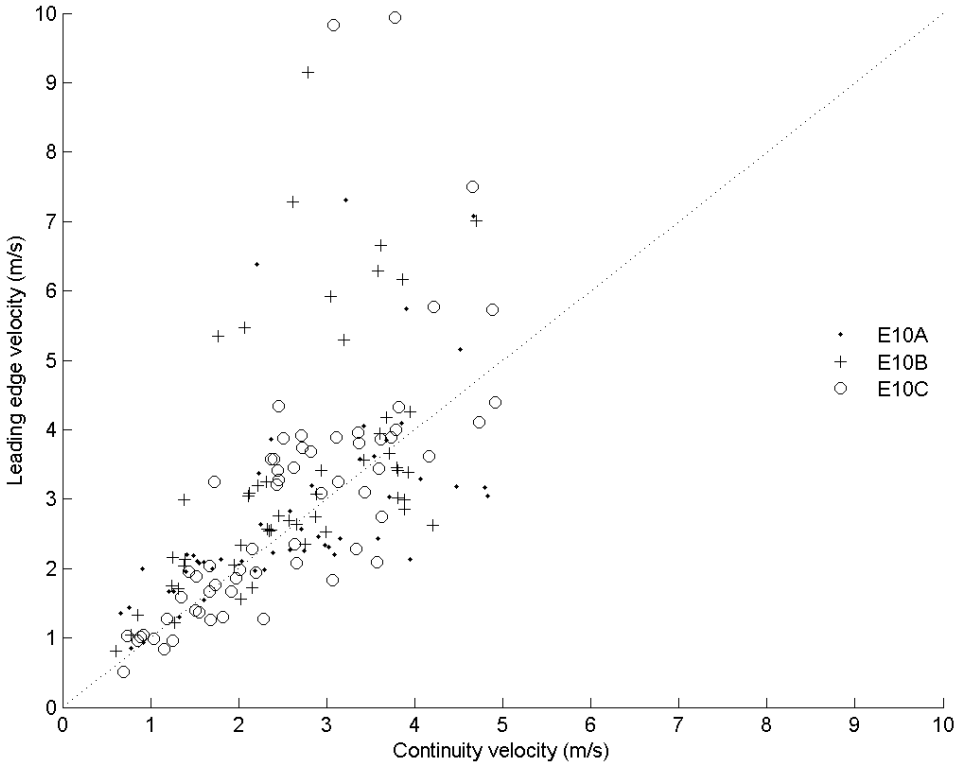

825

826 Figure 4. A comparison of velocity estimates using the continuity and leading edge

827 techniques. The equality line is represented with a dashed-line.

828

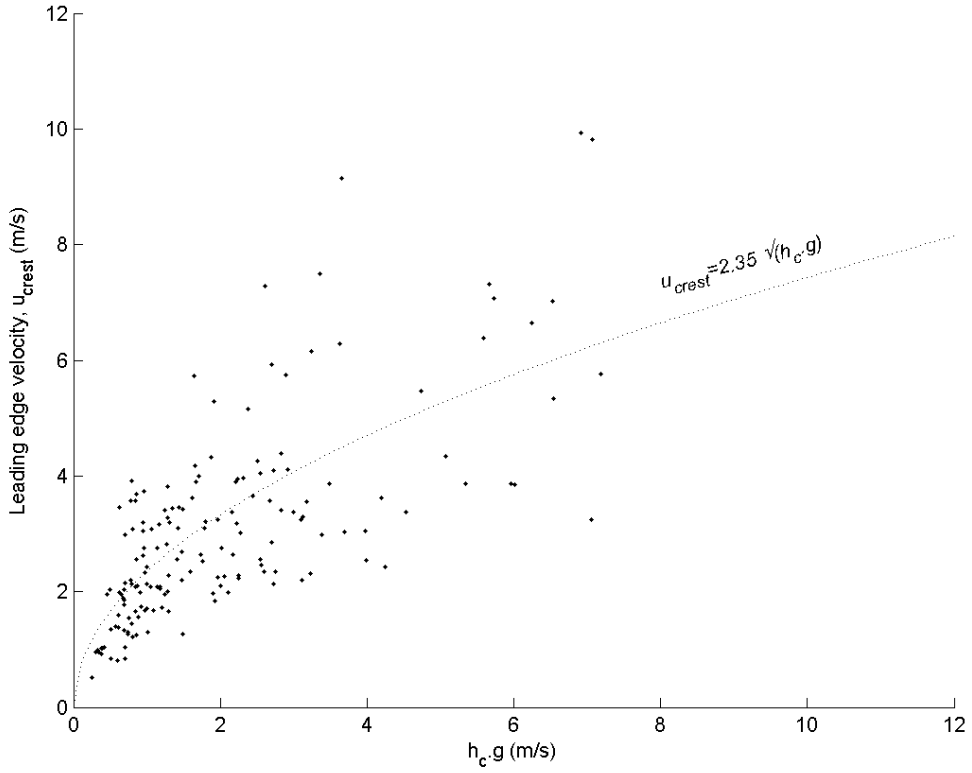
Leading edge velocity, u_{crest} (m/s)
$h_c.g$ (m/s)
$u_{crest}=2.35\sqrt{(h_c.g)}$
0
2
4
6
8
10
12

829

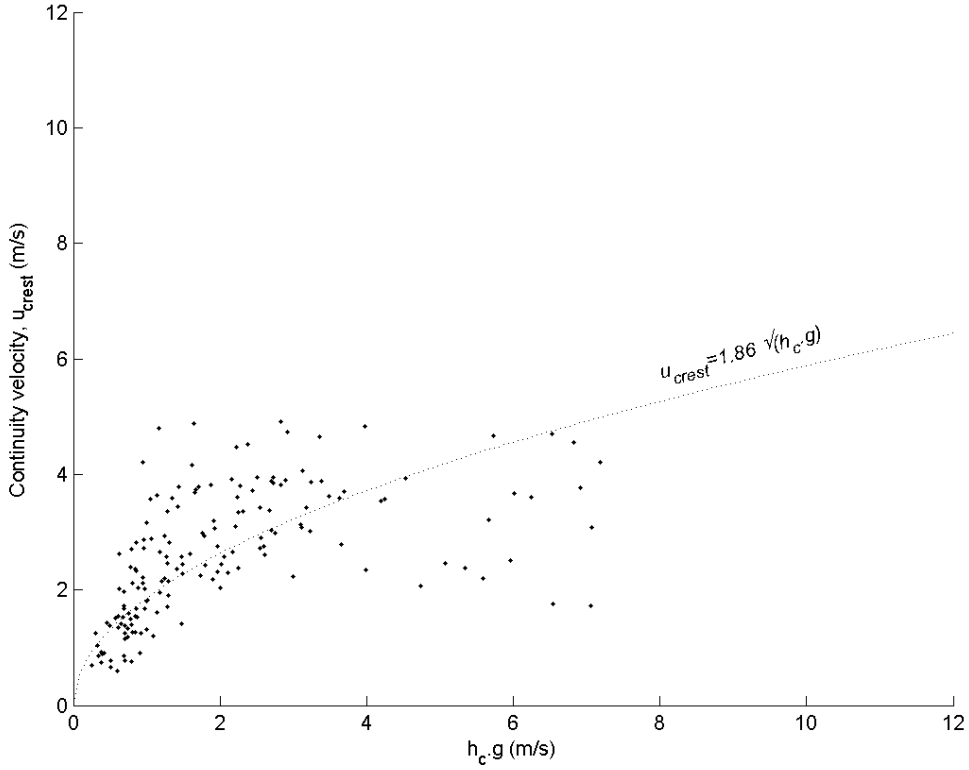
Continuity velocity, u_{crest} (m/s)
$h_c.g$ (m/s)
$u_{crest}=1.86\sqrt{(h_c.g)}$
0
2
4
6
8
10
12

830

831 Figure 5. (a) Overwash leading edge velocity at crest (u_{crest}) as a function of
832 overwash depth at the crest (h_c)*gravitational acceleration (g). The line of power
833 fitting adjustment to data is represented with a dashed-line. (b) Overwash
834 continuity velocity at crest (u_{crest}) as a function of overwash depth at the crest
835 (h_c)*gravitational acceleration (g). The line of power fitting adjustment to data is
836 represented with a dashed-line.

837

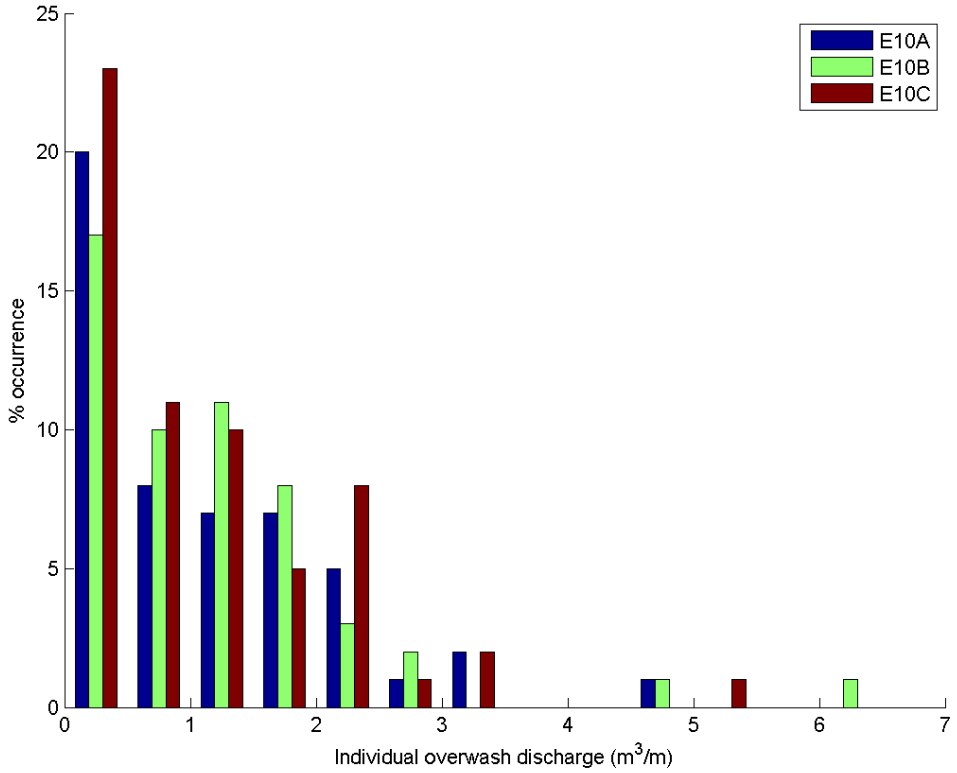

838

839 Figure 6. Percentage of occurrence of overwash event discharge over the barrier
840 crest for all events of Test Series E10A, E10B, and E10C.

841

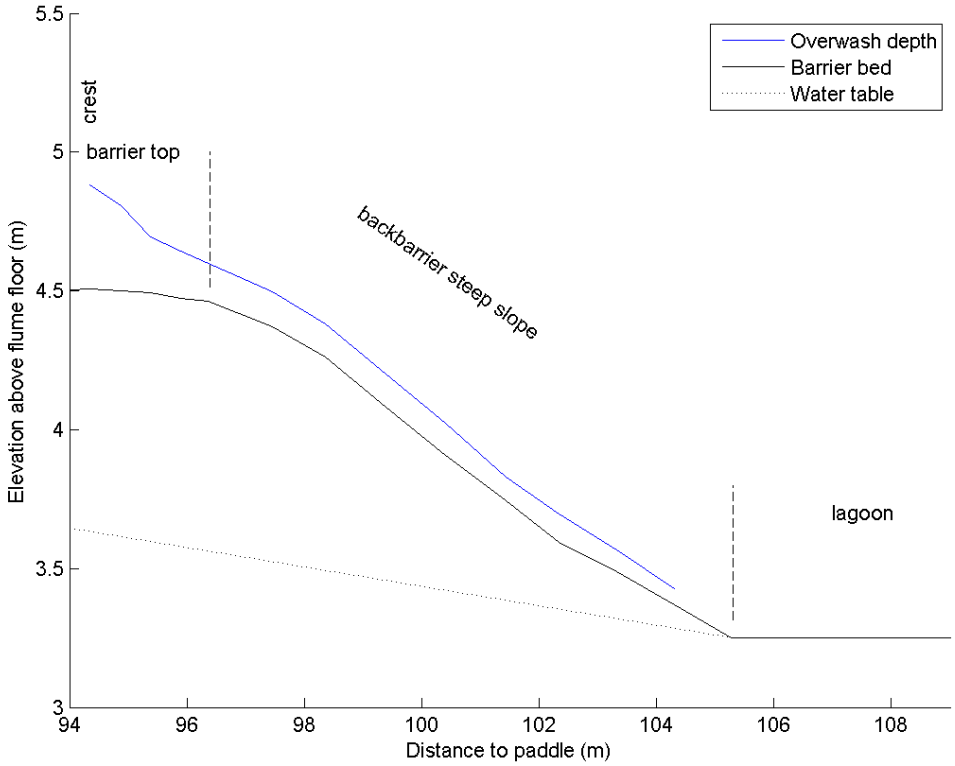

842

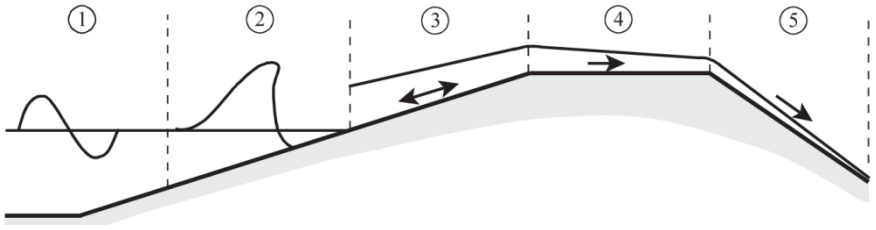

843

844 Figure 7. (a) Barrier cross-shore profile from the crest to the lagoon, and mean
845 peak overwash depth across the barrier, considering only overwash events from
846 E10A, E10B and E10C that reached the barrier lagoon edge (BLS 44; 104 m from
847 paddle). (b) Schematic representation of a sea dyke and the flow domains: 1 – toe
848 of the dike; 2 – wave breaking zone of the seaward slope of the dike; 3 – seaward
849 slope of the dike; 4 – dike crest; 5 – landward slope of the dike (from Schüttrumpf
850 and Oumeraci, 2005).

851

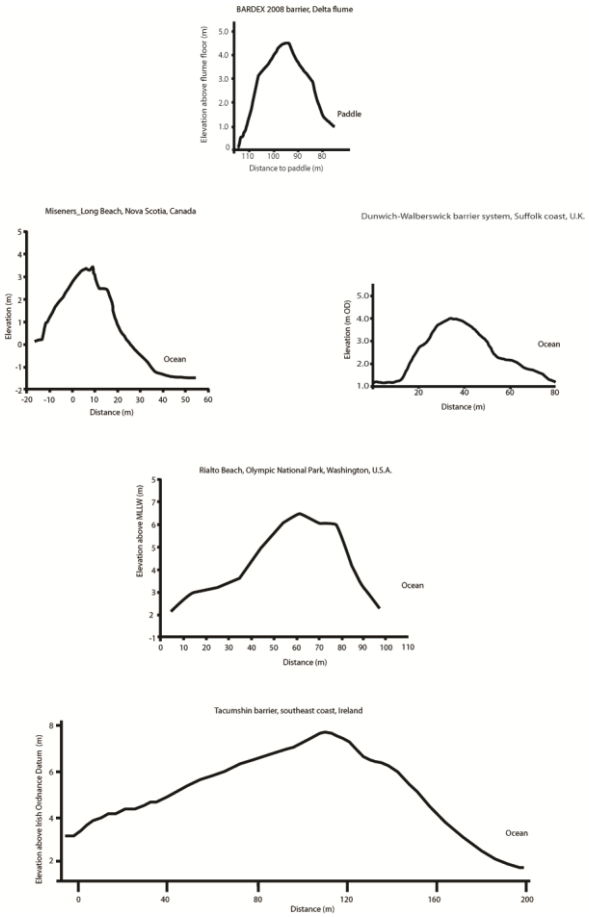

852

853 Figure 8. Cross-shore barrier profile from Test Series E10A of BARDEX experiment
854 compared to gravel barrier profiles from several sites: Miseners Long Beach, Nova
855 Scotia, Canada (adapted from Taylor et al., 1997), Dunwich-Walberswick barrier
856 system, Suffolk coast, U.K. (adapted from Pye and Blott, 2009), Rialto Beach,
857 Washington, U.S.A. (adapted from McKay and Terich, 1992); Tacumshin barrier,
858 southeast coast, Ireland (adapted from Orford et al., 1988). All profiles are
859 represented at the same scale.

860

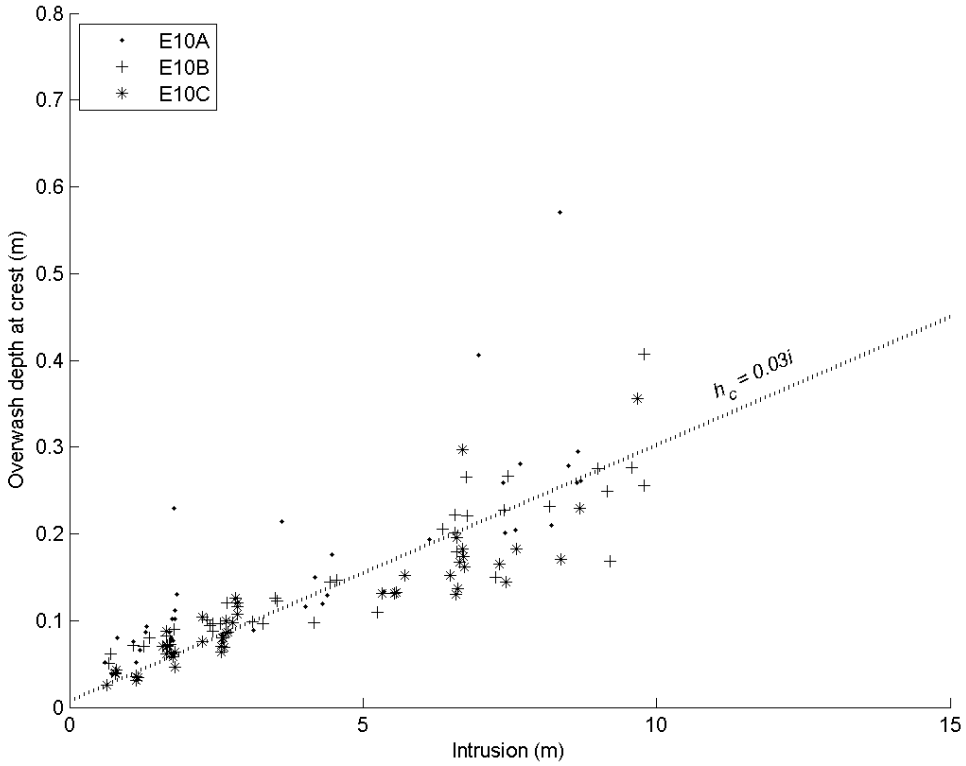

861

862 Figure 9. Overwash depth at the crest (h_c)as a function of overwash intrusion (i). A
863 linear fit to the data is represented with a dashed-line. The fitting equation was
864 obtained excluding data with intrusion>9.8 m (distance between the barrier crest
865 and the lagoon).

866

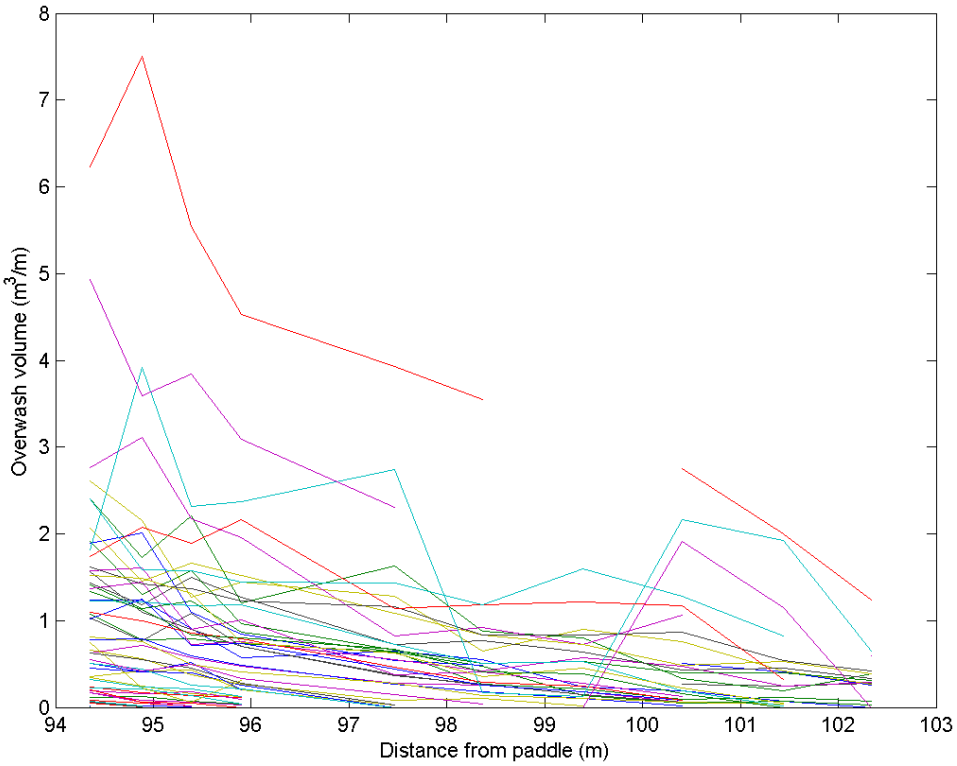

867

868 Figure 10. Total overwash flow volume per event across the barrier top and

869 backbarrier, for all overwash events of Test Series E10B.

870

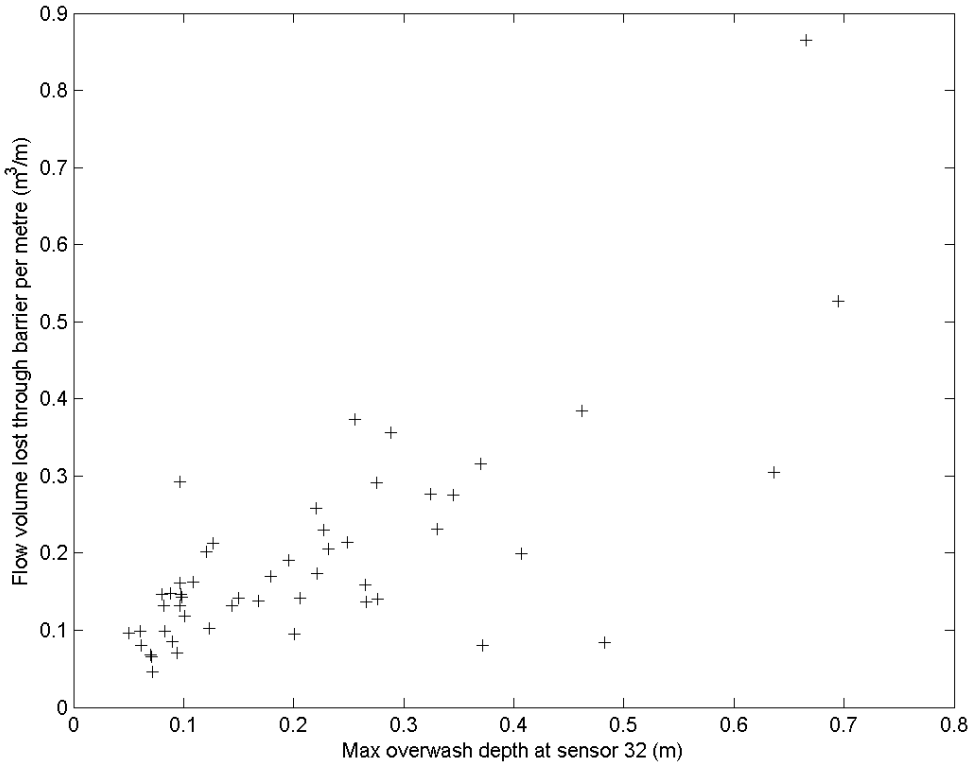

871

872 Figure 11. Overwash flow infiltration through the barrier as a function of peak

873 overwash depth at the barrier crest (h_c).

874

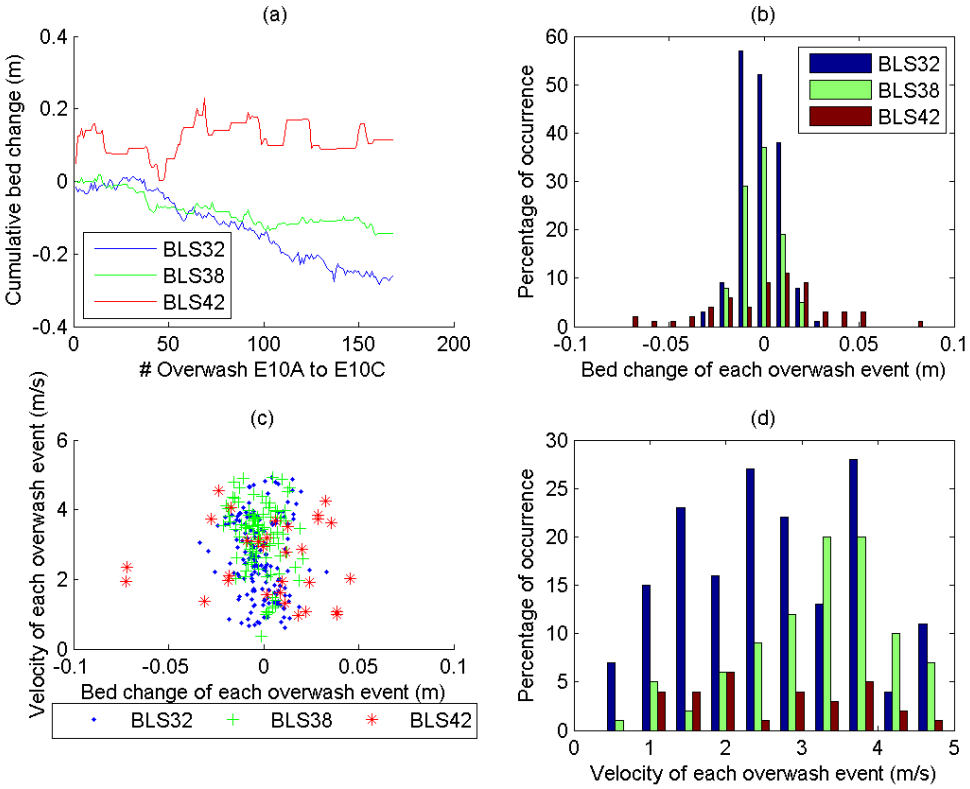

875

876 Figure 12. (a) Cumulative bed level change after overwash events from the
877 beginning of E10A until the end of E10C, at the barrier crest (BLS32), barrier top
878 (BLS38) and backbarrier region (BLS42). (b) Percentage of occurrence of bed
879 erosion (negative) and bed accretion (positive) for each overwash event of Test
880 Series E10A, E10B, and E10C. (c) Bed level change versus overwash velocity for
881 every overwash event at the barrier crest (BLS32), at the barrier top (BLS38) and
882 backbarrier region (BLS42). (d) Percentage of occurrence of continuity velocity for
883 all overwash events of Test Series E10A, E10B and E10C.